ISBN: 978-3-95450-234-9 ISSN: 2673-5504 doi:10.18429/JACoW-SRF2023-FRIBA02

INSTRUMENTATION FOR HIGH PERFORMANCE CAVITIES AND CRYOMODULE FIELD EMISSION ANALYSIS

G. Devanz, E. Cenni, O. Piquet, M. Baudrier, L. Maurice
CEA Université Paris-Saclay, Gif-sur-Yvette, France

Abstract

Field emission (FE) is one of the main reasons for the degradation of accelerator cryomodules, as field emitted current tends to become more severe during the beam operation. It is essential to better understand how this phenomenon is generated and evolves from the SRF cavity preparation in the clean room, through their assembly in the cryomodule until their final test and operation. Due to the shielding environment of a cavity in its vertical test stand, or the architecture of a cryomodule, the more faint radiation occurring at the FE onset remains undetected. More precise diagnostic and analysis tools are required to gain more information. We present the development of dedicated time-resolved detectors for the FE radiation which aim to improve its coverage in terms of solid angle and lower energy threshold sensitivity. We approach this topic through detailed simulation based on the Geant4 toolkit in order to analyse the interaction of FE radiation with the cavity environment and optimize the detectors with respect to their application in cryomodule or vertical test stands. We illustrate this by analysing recent cryomodule experimental test data.

INTRODUCTION

State of the art cavity preparation and clean room assembly techniques enable individual multi-cell, elliptical cavity field-emission-free performance. Large projects generally choose to minimize the amount of time dedicated to the HPR for a given pass rate on the first RF test of a cavity. Then a new treatment is applied to the field emitting cavity. A high rate of typically 90% is then achieved. The remaining cavities are then dealt with on a case-by-case basis due to diminishing returns.

When the FE-free, vertically tested cavities are assembled into a string, keeping the same level of cleanliness for the assembled cryomodule (CM) is obviously a challenge. First, new parts such as bellows, power couplers and gate valves are now connected to the beam vacuum. Particle counting is the tool of choice to guarantee that the level of cleanliness of the parts will not contaminate the cavity surfaces. Despite all assembly with backflow, evacuation, venting, connections to vacuum pumps and other processes being kept under tight control, the FE threshold is often brought back within the range of cavity operation gradient.

Testing individual cavities within the CM can inform on the possible impact of vacuum equipment connection if end cavities experience a reduction in performance. The test can inform only on a basic level whether the cavity performance is retained or degraded.

Only the absence of FE is a strong proof that the assembly has reached its goal. In the opposite case, one has to compare two FE measurements done in different contexts and available instrumentation:

-Various shielding situations: The nature and quantity of shielding material between the cavity and the radiation monitors differ from one test infrastructure to the next, and from a vertical test (VT) to a cryomodule test.

- Different radiation monitors,

- Mode of operation: pulsed instead of continuous may introduce an excursion from the linear response of a detector due to its intrinsic dead time. Geiger-Müller (GM) and neutron rem counter are subject to this limitation generating a saturation at higher count rates [1].

A fair comparison between VT and CM tests is possible if one ensures that both situations have used the same measurement equipment. This is one strong motivation to develop a radiation instrumentation that could be used in both cases and installed at the same relative position with respect to the cavity. If the radiation sensitive part of the detection is taking place at cryogenic temperatures, and should be even placed in liquid He directly to be able to cover all the use cases.

A limitation of standard area radiation monitors, GM or ionization chambers is their size which makes it very difficult to imagine a tight coverage in terms of angular distribution around the cavity under test. In a VT test case, they would be installed around the Dewar in room temperature conditions, separated from the source by shielding material. VT setups generally do not include more than two or three monitors, while this number can be increased to more than 10 units in a CM test bunker.

Area radiation monitors, GM or neutron rem-counters measure the ambient dose equivalent H*(10). The conversion between the equivalent dose and neutron flux requires Monte-Carlo (MC) simulations, since the equivalent dose depends on an energy-dependent weighting factors. Using data from [2] makes evaluating the neutron flux from H*(10) measurements possible under the hypothesis of a neutron energy spectrum.

Improvements over standard area monitors would be the access to timing information and energy of the radiation. Then combining measurements with MC simulations makes it possible to identify an electron emission scenario and potentially track back to the initial electron current.

During the ESS elliptical cavity CM tests at Saclay [3, 4] and Lund Test Stand (TS2) [5], the false triggering of the power coupler arc detection interlocks with γ radiation occurred multiple times. The time resolved detection of the radiation can provide useful information to inject into the interlock system logic. It can also enable the disambiguation of different origins of the measured radiation in pulsed operation.

ISBN: 978-3-95450-234-9 ISSN: 2673-5504 doi:10.18429/JACoW-SRF2023-FRIBA02

DETECTION OF GAMMA RADIATION

Our developments are focussed around plastic scintillators which offer a number of interesting properties namely time response of a few nanoseconds, capability to be machined or formed in any shape, including fibres or light guides, and low cost. The latter opens to the possibility to cover a large surface area or angle coverage for γ detection combined with the potential to collect the scintillation light at discrete positions with a photo-detector, possibly remote from a harsh environment, in our case liquid helium and high radiation flux. A number of examples of the use of plastic scintillators exist, including in high radiation exposure areas around LHC detectors (LHCb SciFi tracker [6]).

The measurement unit setup consists of a scintillating material in our case Polyvinyltoluene (PVT), an optical light collection system that transfers the optical photons to the photodetector, the readout electronics and a data acquisition system. For the first tests the scintillating fibre was directly connected to a Hamamatsu H10720-110 photomultiplier tube (PMT) read by an all-analogue electronics with a 10 µs integrating amplifier. The integration time was originally chosen for the fast arc detection interlock system for the power couplers (FPC). The time variation of the γ radiation signal can be recorded by any DAQ system, and already helps identify if the origin of the radiation is FE, i.e. the intensity varies in conjunction with cavity gradient, FPC electron emission if it is synchronized with e^- detection in the FPC, or multipacting (MP) in the cavity.

An alternative is to choose the photon counting mode by connecting the PMT anode to a high bandwidth trans-impedance amplifier (TIA) in order to change the fast PMT anode photocurrent into voltage. If connected to a matched transmission line it is then possible to obtain voltage pulses of a few ns each time a photon or a group of coincident photons are detected by the PMT. The Hamamatsu C5594 amplifier we used has a bandwidth of 1.5 GHz. With this setup it becomes possible for each group of coincident photons to obtain a voltage pulse proportional to their number. The principle of γ spectroscopy with scintillators relies on the fact that one γ generates a number of scintillation photons in the material which is proportional to its energy. Keeping a linear relationship between the number of detected photons in the PMT and the height of the voltage pulse at the output of the TIA is then a way to obtain the primary energy information. The proportionality constant relating the voltage to the energy is obtained through calibration with a known radioactive γ source. The limitation of this idealized situation starts with the fact that the incoming γ does not release all its energy into scintillation photons. In the case of fibres, the probability that the γ interacts with the scintillator material is already low because of the density and size of the fibre. However, the γ emission rate in a cavity with FE or MP makes up for this as will be demonstrated.

We performed initial testing of a single 1.5 m long fibre equipped with a PMMA optical fibre at each end to guide the scintillation photons out of the VT Dewar, as represented in Fig. 1. It has been used for 4 vertical tests of β=0.86 ESS cavities [7] at the temperature of 2 K.

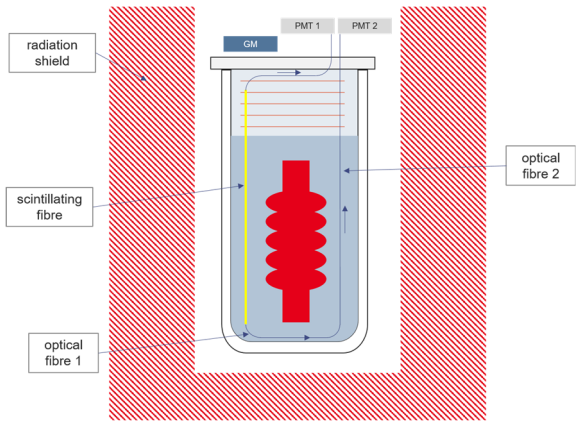

Figure 1: Single PVT fibre test in the VT cryostat.

The scintillation photon count rate is compared to the dose rate measured on the top plate of the VT insert using a GM tube in Fig. 2 while testing a contaminated cavity. The recording of the PMT signal starts at 14:08. The cavity quenches at 15:18 before E_{acc} was recorded, which explains the presence of scintillation counts on the right side of the plot.

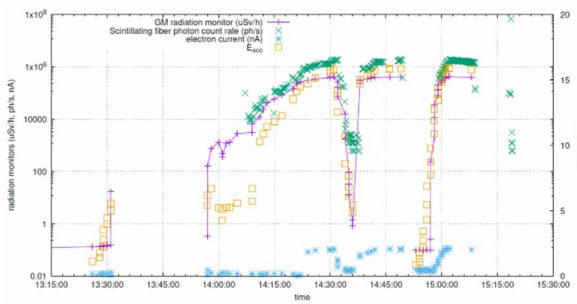

Figure 2: Radiation measurement on the contaminated HB08 cavity before re-retreatment.

The PMT signal was repeatedly recorded using an oscilloscope at a sampling rate of 5 GHz and a sampling time of 200 µs. The data were processed offline to obtain the PMT pulse count. The count rate obtained with the fibres follows the measured dose rate. After selecting two sets of scintillation signal recordings for which the gradient was stabilized respectively at 11.8 and 15.9 MV/m, the PMT pulse height distribution was analysed. The resulting histograms are displayed in Fig. 3. The pulse height distributions for the two cavity gradients clearly differ by their maximum voltage range. This confirms the pulse height data carries information about the energy spectrum of the γ radiation. This is a preliminary test of the potential use of the fibres as an energy discriminator if an additional step of calibration is performed with a known γ source.

ISBN: 978-3-95450-234-9 ISSN: 2673-5504 doi:10.18429/JACoW-SRF2023-FRIBA02

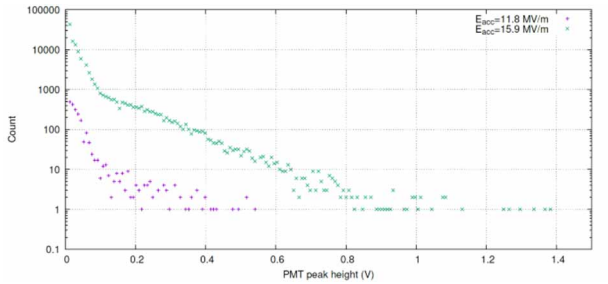

Figure 3: Pulse height histogram of scintillation at 11.8 and 15.9 MV/m.

The next step is to extend this single detection unit to build a small scale multiple fibre system for the 1.3 GHz single-cell VT arranged in a birdcage-like configuration around the cavity as shown in Fig. 4. Our objective is to cover most of the angular distribution of radiation around the cavity and evaluate the sensitivity of the fibre net to inhomogeneity of the radiation pattern. The only detector parts visible are the vertical and horizontal PVT fibres in this Geant4 [8] model. The current design discussed below comprises 52 channels so multichannel photo-detectors like MPPCs will be used instead of PMTs.

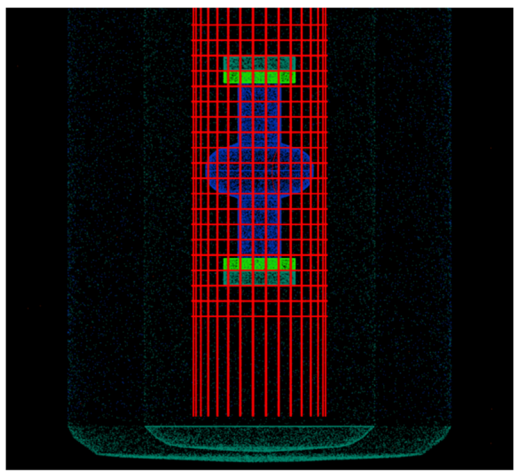
Figure 4: Layout of the single-cell VT prototype radiation detector.

GEANT4 MODELLING

Geant4 models have been developed in order to have a tool to both simulate the FE-induced radiation optimize the arrangement of a number of detectors for the various RF test cases and simulate our measurements to help their analysis. We modelled the CEA single-cell vertical test setup and the ESS HB CM in its test bunker, both for Saclay and ESS Lund sites.

Physics Modelling

Accelerated electrons hit the beam vacuum boundary, producing ionisation and bremsstrahlung in the Nb or stainless steel boundaries of the beam vacuum. The γs experience scattering in the material layers they travel through and may interact with one fibre. From the outside of the cavity we mostly expect to detect γs that follow an energy spectrum typical of Bremsstrahlung. Scattering inside the cavity can lead to the generation of new electrons or positrons far away from the original FE source location.

All simulations have been performed with the EM option 4 since in our case we are mostly dealing with low energy electromagnetic processes. Depending on the studied case, we include optical physics (scintillation, Cerenkov radiation and optical photon propagation), high-precision neutron physics, or both.

Our first simulation procedure consisted in a first computation of FE electron trajectories from the surface with a combination of Superfish and Fishpact [9]. The 2D simulation is fast and provides a mapping from an emitter to the impact point and energy. Then a Geant4 simulation would be run for a set of impacts determined by their position and electron momentum at the impact point.

Improved Modelling with Tracking of Primaries and Secondary Particles in the EM Field

The specific interaction of a charged particle with a RF field is not directly included in Geant4 but the pre-existing coding of the particle tracking inside a magnetic field can be extended to achieve this. The Geant4 toolkit includes tracking integrators that allow for a 6-component field, three of which are allocated to the 3D components of B, the remaining ones corresponding to E. Our developed G4 application features the import of a 3D Cartesian RF field map, dynamic evaluation of the field components with an interpolation routine and tracking inside the RF field. This enables us to model most of the studied cases by defining the initial electrons emission location and timing. The electron is tracked and accelerated in the RF field, so it can be generated at very low initial energy. In addition, a specific particle generator has been included to model the FE time-dependent intensity. For a given gradient in the cavities set at the start of the run, the relative probability for an electron to be emitted at a given RF phase has been made to follow the RF Fowler-Nordheim law coded with a Monte-Carlo routine.

SINGLE CELL CAVITY SIMULATIONS

The VT tests are mostly carried out in CW mode. Let's evaluate the simple case of a single electron being emitted at each RF period at the iris of a single cell 1.3 GHz cavity running at 30 MV/m. The average FE current is then 0.2 nA. In this case, the simulations confirm that typically 10^8 γ are released each second outside the cavity volume in 4π sr. The scintillation rate of photons detected at a single vertical fibre end ranges typically from 10^3 to 10^5 s^{-1} depending on its position around the cavity. This high count rate has also been obtained during the tests of HB08, so we are confident that the required integration time will be within seconds. A set of simulations has been performed to determine an arrangement of fibres around the cavity as depicted in Fig. 4. A combination of 32 vertical fibres and 20 equatorial fibres was found adequate for the coverage of all but top and bottom directions. An example of the simulated resulting interaction of the radiation with the fibres

ISBN: 978-3-95450-234-9 ISSN: 2673-5504 doi:10.18429/JACoW-SRF2023-FRIBA02

is shown in Fig. 5. The histograms report the count of detected scintillation photons by each vertical and horizontal fibre. The combination of histograms gives the position of the peak and spread of the spatial distribution of the radiation.

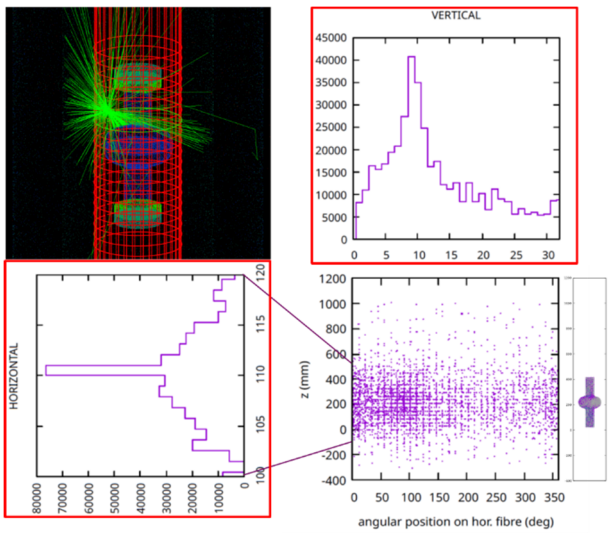

Figure 5: Simulation of the scintillation photon generation and collection, the histogram represents the photon count on each vertical and horizontal fibre.

The lower energy γs have a more uniform angular distribution due to larger scattering angles than higher energy γs. Using a threshold on the height of the peaks counted on each fibre will provide a way to keep only counting events of higher energy γs, therefore, reduce the smearing of the horizontal and vertical angle distribution.

To detect the radiation emitted closer to the vertical direction, two scintillator disks will be placed above and below the cavity (not shown). This way the number of additional readout channels is kept low.

CRYOMODULE TEST SETUP

In the case of a multiple cavity cryomodule in a test bunker environment, it is of interest to check whether the cleanliness of the cavity has been preserved from the vertical test to the final assembly of the CM. Even when testing a single cavity at a time, multiple radiation monitors are required to cover the radiation field inside the bunker. In this paper, we discuss only ESS medium and high β elliptical cavity CM tested at Saclay, summarized in [10].

An important difference with the single-cell cavity is the extended impact energy range of the FE electrons, reported in Table 1 for the ESS elliptical cavities.

The geometrical β of 0.86, optimal β of 0.92 and large iris diameter of 120 mm of the high β create favourable conditions for electron acceleration across several cells.

During tests of ESS cryomodules up to 9 GM tubes, one rem-type neutron detector were used simultaneously. During pulsed cavity operation the RF pulse structure is ranging from 300 μs, 1 Hz to 3.6 ms 14 Hz, approximately 5% duty cycle (d.c.).

Table 1: Impact Energies Ei for ESS Cavities

Beta			**0.67**	**0.86**
Eacc [MV/m]	from	to	16.7	20
Most probable				
Ei [MeV]	3rd iris	out	7.5	7.3
	3rd iris	same cav.	1.6	1.1
	4th iris	out	6.6	12
	4th iris	same cav.	1.5	1.1
Max. Ei [MeV]			7.7	15.2

The GMs are covering two dose rate ranges. The lower range is rated up to 1mSv/h, and the higher range up to 1 Sv/h for continuous mode. The low dose type was able to discriminate low activity but was exchanged when possible with high dose one, because of their early saturation due to dead time. In the 5% d.c. pulse mode the maximum dose rate is divided by 20 compared to the range specified for CW. The minimum time between two discharges in the tube is the source of the limitation of the GM. We also reached the saturation of the high dose GMs for several cavities during the tests of eight ESS CMs at Saclay. In this case the maximum dose rate recorded was 10 mSv/h.

Two 2-inch NaI(Tl) based spectrometers were used throughout all tests performed. The main objective is to evaluate the end energy of the Bremsstrahlung spectrum. This is an important value when discriminating between emission scenarios. When a cavity reaches its nominal gradient, in most cases this end energy is in excess of 7 MeV.

The calibration of GMs is performed with a ^{137}Cs source emitting at 661 keV and no calibration data is available from the manufacturer above 1.3 MeV. Therefore, in a radiation field with γ energies reaching up to 15 MeV, GMs provide only the order of magnitude of the equivalent dose rate. One should restrict their use to confirm the good performance in terms of FE of cavities, to compare the performance of a set of identical cavities, or monitor the evolution of MP processing in a cavity.

Geant4 Model

A graded realism approach has been chosen for the geometrical representation of the CM owing to the high count of components. A high level of detail is kept for cavities, vacuum parts of the FPCs and beam vacuum components (Figure 6).

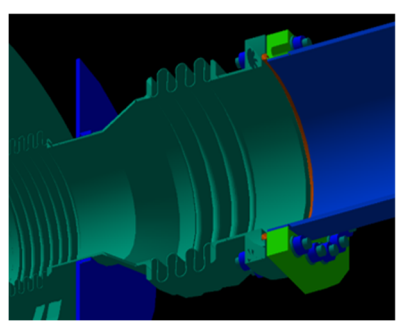

Figure 6: Highly detailed area of the Geant4 model.

ISBN: 978-3-95450-234-9 ISSN: 2673-5504 doi:10.18429/JACoW-SRF2023-FRIBA02

Then, details of the thermal shield, the space frame and the vacuum vessel are ignored based on their size, mass or distance from the beam axis (Figure 7).

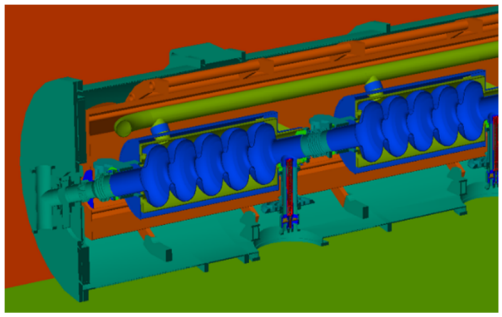

Figure 7: Reduced detail level of the ESS CM Geant4 model for components surrounding cavities.

Material properties used in the simulation reflect the real chemical composition as closely as possible by using the data provided by the material certificates of the manufactured components.

CM31 Neutron Emission Analysis

One of the FE scenarios encountered during the high power test of the cavity 4 of CM31 has been analysed with greater detail, after the neutron dose rate of 400 µSv/h was detected on the LB6411 rem counter installed inside the test bunker. The cavity was operated at nominal gradient and duty cycle. After the CM31 test and access to the cold mass, the main location of the activated area was found on the beam tube of the cavity 3 at the longitudinal position of the tuner. The nature of the activated material was found by measuring its γ decay at 935.44 keV with a half-life of 10.2 days. The corresponding radio-element is ^{92m}Nb. The scenario explaining this result requires bremsstrahlung γs to excite stable Nb nuclei into giant dipole resonance (GDR). The outcome is the emission of neutrons before the resulting ^{92m}Nb decay. The GDR cross section is maximum at 16.2 MeV for ^{93}Nb [11]. The threshold for the (γ,n) reaction is 8.9 MeV. Given the value of E_{acc} at 20 MV/m, the electron trajectories computation narrowed down the possible location of the FE emitter to the iris between cells 1 and 2 of cavity 4 [12]. The highest impact energy is obtained for the electron transmitted to the next cavity, up to 15 MeV in this case. Geant4 simulations were then performed to evaluate the simplified scenario by which mono-energetic 15 MeV electrons impact cavity 3 beam pipe with a shallow angle of 2° as prescribed by the Fishpact trajectory simulations.

We expect GDR to produce neutrons with a Maxwellian energy spectrum. One simulated neutron spectrum for a mono-energetic 15 MeV electron beam hitting cavity 3 is displayed on Fig. 8 along with a Maxwellian distribution with a temperature of 0.43 MeV.

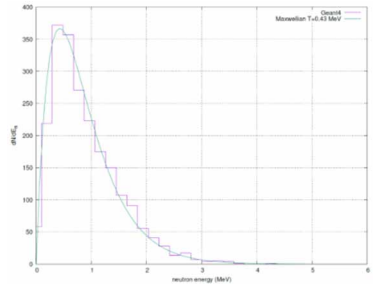

Figure 8: Simulated neutron energy spectrum originated by Nb GDR.

The Geant4 simulation was used to estimate the distribution of the generated neutrons along the cryomodule axis (Figure 9). This was a hint that the first activated spot was only accounting for one half of the total induced activity, the other half being spread along cavity 2. This is explained by the scattering of primary electrons on the beam pipe of cavity 3 as can be seen in Fig. 10.

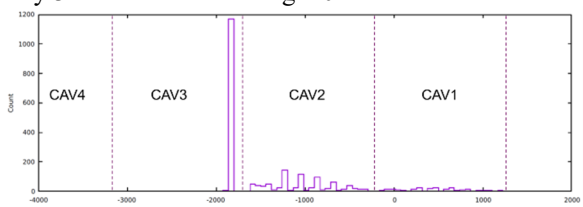

Figure 9: Generated neutron distribution along the CM axis.

In this simulated case, 87% of electrons hitting cavity 3 are scattered, and 63% impact cavity 2 with an energy above 8.9 MeV, so still candidates for the production of bremsstrahlung γ at the (γ,n) threshold in Nb.

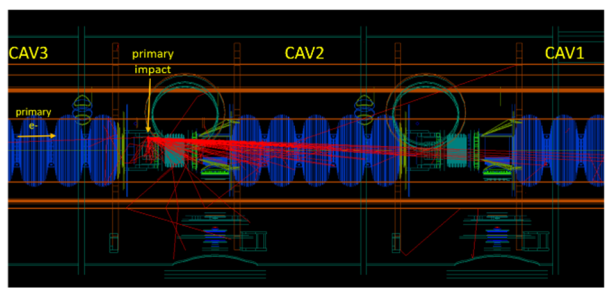

Figure 10: Scattering of 15 MeV electrons impinging on cavity 3.

Typical neutron trajectories inside the test bunker are shown on Fig. 11 as coloured lines.

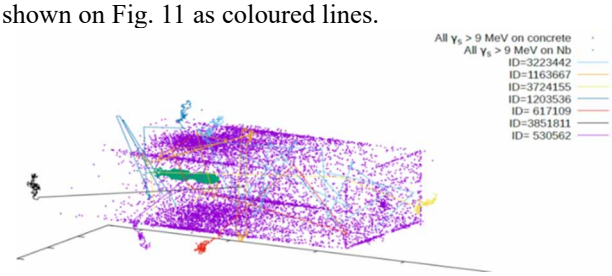

Figure 11 Example of typical neutron trajectories in the test bunker.

ISBN: 978-3-95450-234-9 ISSN: 2673-5504 doi:10.18429/JACoW-SRF2023-FRIBA02

The CM test bunkers at CEA or ESS do not contain moderating materials on the walls, so neutrons experience a number of scattering processes before being stopped either in the walls or in the detector, creating this bouncing-like behaviour. This, added to the isotropic generation of the neutrons makes the placement of the detector within the bunker not very critical. The fraction of detected neutrons by the monitor is obtained by simulation.

The next step was to perform a full simulation with the improved Geant4 modelling described earlier in this paper. The input parameters are the position of the emitter, the gradients in each cavity and the parameters of the Fowler-Nordheim law (enhancement factor and work function). The main difference with the mono-energetic case is that the electron impact energies on the beam vacuum boundaries now follow a complex distribution (Fig. 12).

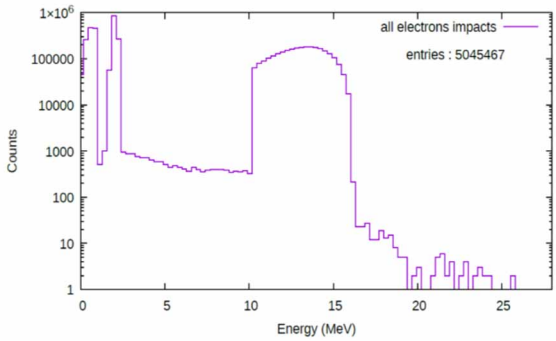

Figure 12: Simulated impact energy spectrum of FE electrons from cavity 4 at a gradient of 20 MV/m.

The net effect is that the neutron yield (η) per generated electron is significantly reduced with respect to the mono-energetic model by a factor of 4.6 at 1.21 10^{-5}.

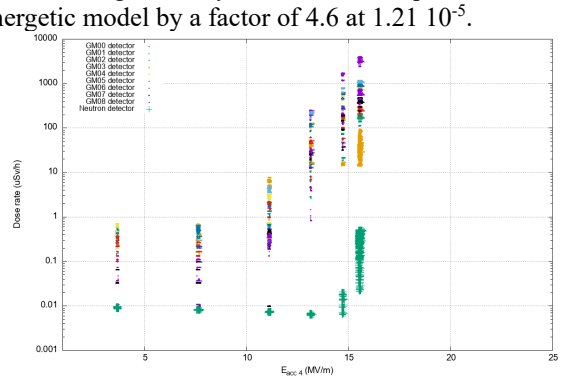

Figure 13: CM31 dose rate measurement with GM tubes and neutron dose rate near the neutron emission threshold for cavity 4.

Experimentally neutron counting started at a gradient of 14.7 MV/m as shown in Fig. 13. Simulation have been performed by launching electrons from the same FE emitter, scanning the accelerating gradient of cavity 4 from 14 to 22 MV/m. The neutron yield per electron is computed for each gradient, no assumption is needed concerning the FE current. We simply know from GM measurements that the FE onset is between 10 and 11 MV/m for cavity 4. Therefore, we interpret the neutron emission at 14.7 MV/m as the threshold at which the neutron yield stops being zero experimentally. No biasing was used in the simulation so the statistics near the threshold could be improved, but the calculation already agrees with experimental data and confirming of the validity of the G4 model.

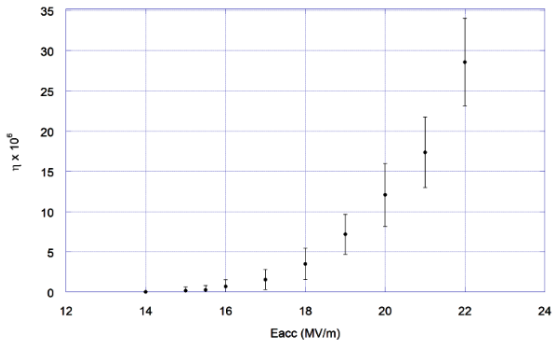

Figure 14: Geant4 simulation of the neutron yield per generated electron as a function of cavity 4 gradient.

We have two sources of data to estimate the number of neutrons generated in Nb during the 5 hours of the cavity 4 operation at the nominal gradient, one derived from the rem counter integration and the other derived from the estimation of Nb activation. The estimate of the average FE current during the flat top of the cavity (3.25 ms) obtained from these two sources and the neutron yield per electron from our Geant4 models ranges from 4 to 18 μA for the mono-energetic model and from 10 to 44 μA for the improved model.

Time Domain Radiation Measurements

The counting operation can be gated on the MCA of the spectrometers, which introduces the possibility to perform radiation measurements during time slices of the RF pulse. This capability was used during the test of CM01 to determine that the radiation observed when operating cavity 4 was emitted for two short periods a few tens of μs only in duration, one at the end of the filling time and a second during the decay of the cavity, around a specific value of the reflected power. This could be positively correlated with the electron pickup signal recorded during the pulse with a typical resolution of 10 μs. This type of behaviour was observed multiple times across MB and HB CM tests. The PVT scintillator fibres and blocks have been used for later tests to provide time resolved radiation measurements as described in [13].

The specific scenario of a short radiation burst has been partially modelled with Geant4 for the HB modules. Runs were performed launching electrons from the coupler port on the cavity side with a random momentum direction, but within the range of kinetic energy of MP electrons in the ESS couplers (from 10 eV to 1 keV) while the cavity field has started to decay after the RF pulse (typically at values around 14 MV/m in the HB cavity). As shown in Fig. 15, a subset of these electrons are captured by the cavity mode and accelerated to a restricted region on the first cell side wall. The impact energy is of the order of 1 MeV. Backscattered electrons are then emitted, some of them with the

ISBN: 978-3-95450-234-9 ISSN: 2673-5504 doi:10.18429/JACoW-SRF2023-FRIBA02

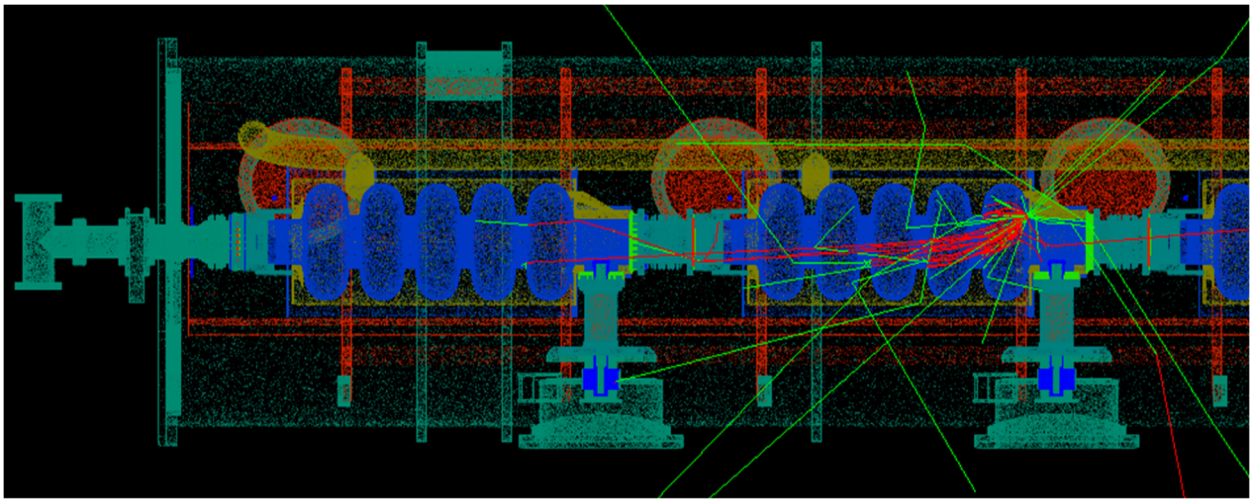

Figure 15: Example of electron and γ trajectories initiated by electrons emitted with an initial energy of 100 eV from the coupler port captured by cavity 2 field during decay at a random RF phase.

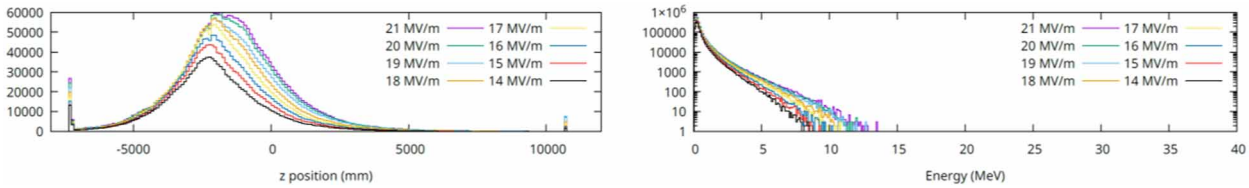

Figure 16: Simulation of radiation in the bunker (left along the beam axis, right energy spectrum) in the case of the CM31 FE scenario in cavity 4.

phase and momentum conditions such that they are either accelerated and exit the cavity or scattered once or several times more. The whole process takes a few RF periods, so the gradient in the cavity can be considered constant

Distribution of Radiation in the Bunker

Prediction of the radiation pattern and energy spectrum inside the test bunker is a natural application of the improved Geant4 model. Using the neutron emission scenario linked to FE in cavity 4 of CM31 as a starting point, we can simulate a several useful data. The left side of Fig. 16 represents the distribution of γ radiation along the beam axis in the test bunker for a range of gradients, integrated on the transverse directions. This informs us that the scale of the features of the distribution is about 1 m and how to distribute radiation monitors in the bunker to capture these details. On the right side of Fig. 16 is represented the gamma energy spectrum outside at the level of the bunker walls that we can expect to measure.

CONCLUSION

We have investigated the possibility to develop and use specific scintillator-based radiation detectors in addition to the usual area radiation monitors. The time resolution they provide considerably improves the capability to track the origin of the radiation. The development of a simulation tool using the Geant4 toolkit besides being indispensable to design and optimize the new detectors provides not only a help for measurement analysis but also a predictive insight.

The pulsed radiation behaviour of ESS elliptical cryomodules still needs to be studied. In this paper we have only described cases related to single cavity operation. We could relate the neutron and activation measurements with a FE current using simulation. The extension to the analysis of radiation with 4 cavities can be tackled by simulation and experimentally at the Lund TS2, partly with the same tools. One compelling motivation is to understand the interaction of the pulsed parasitic radiation of the CMs with the instrumentation which is foreseen to protect both cryomodule components (e.g. power couplers) and the linac itself.

ACKNOWLEDGMENT

We thank our colleagues of the SRF section at ESS Lund for their support to continue this development.

REFERENCES

[1] M. Caresana *et al.*, "Intercomparison of radiation protection instrumentation in a pulsed neutron field", *Nucl. Instrum. Methods Phys. Res., Sect. A*, vol. 737, pp. 203-213, 2014. doi:10.1016/j.nima.2013.11.073

[2] A. Ferrari and M. Pelliccioni, "Fluence to dose equivalent conversion data and effective quality factors for high energy neutrons", *Rad. Prot. Dosim.*, vol. 76, pp 215-224, 1998. doi:10.1093/oxfordjournals.rpd.a032267

ISBN: 978-3-95450-234-9 ISSN: 2673-5504 doi:10.18429/JACoW-SRF2023-FRIBA02

[3] F. Peauger *et al.*, "Preliminary Test Results of the First ESS Elliptical Cryomodule Demonstrator", in *Proc. IPAC'18*, Vancouver, Canada, Apr.-May 2018, pp. 691-693. doi:10.18429/JACoW-IPAC2018-TUPAF015

[4] O. Piquet *et al.*, "Results of the RF Power Tests of the ESS Cryomodules Tested at CEA", in *Proc. IPAC'22*, Bangkok, Thailand, Jun. 2022, pp. 1186-1188. doi:10.18429/JACoW-IPAC2022-TUPOTK002

[5] C. G. Maiano, "Production, Test and Installation of the ESS Spoke, Medium and High Beta Cryomodules", in *Proc. LINAC'22*, Liverpool, UK, Aug.-Sep. 2022, pp. 685-690. doi:10.18429/JACoW-LINAC2022-TH1PA02

[6] LHCb collaboration, "LHCb Tracker Upgrade Technical Design Report", CERN, Geneva, Switzerland, Rep. CERN-LHCC-2014-001, Feb. 2014.

[7] G. Devanz *et al.*, "ESS Elliptical Cavities and Cryomodules", in *Proc. SRF'13*, Paris, France, Sep. 2013, paper FRIOC02, pp. 1218-1222. https://jacow.org/SRF2013/papers/FRIOC02.pdf

[8] S. Agostinelli *et al.*, "Geant4—a Simulation Toolkit", *Nucl. Instrum. Methods Phys. Res., Sect. A*, vol. 506, p. 250, 2003. doi:10.1016/S0168-9002(03)01368-8

[9] G. Wu, https://Code.Google.Com/Archive/p/Fishpact/.

[10] O. Piquet *et al.*, "Performance Analysis from ESS Cryomodule Testing at CEA", presented at SRF'23, Grand Rapids, MI, USA, Jun. 2021, paper WEPWB064, this conference.

[11] A. Leprètre *et al.*, "The Giant Dipole states in the A=90 Mass Region", *Nucl. Phys. A*, vol. 175, pp. 609-628, 1971. doi:10.1016/0375-9474(71)90454-4

[12] E. Cenni, M. Baudrier, G. Devanz, L. Maurice, and O. Piquet, "Field Emission Studies During ESS Cryomodule Tests at CEA Saclay", in *Proc. SRF'21*, East Lansing, MI, USA, Jun.-Jul. 2021, pp. 677. doi:10.18429/JACoW-SRF2021-WEPTEV016

[13] E. Cenni, M. Baudrier, G. Devanz, L. Maurice, and O. Piquet, "Time Resolved Field Emission Detection During ESS Cryomodule Tests", in *Proc. IPAC'22*, Bangkok, Thailand, Jun. 2022, pp. 1192-1195. doi:10.18429/JACoW-IPAC2022-TUPOTK004